Chemical Science

ROYAL SOCIETY OF CHEMISTRY

EDGE ARTICLE

View Article Online
View Journal | View Issue

Cite this: *Chem. Sci.*, 2021, **12**, 11593

All publication charges for this article have been paid for by the Royal Society of Chemistry

"Click-switch" – one-step conversion of organic azides into photochromic diarylethenes for the generation of light-controlled systems†

Steffy Becht, [a] Reena Sen,[b] Simon M. Büllmann, [a] Andreas Dreuw[b] and Andres Jäschke *[a]

Diarylethenes (DAEs) are an established class of photochromic molecules, but their effective incorporation into pre-existing targets is synthetically difficult. Here we describe a new class of DAEs in which one of the aryl rings is a 1,2,3-triazole that is formed by "click" chemistry between an azide on the target and a matching alkyne–cyclopentene–thiophene component. This late-stage zero-length linking allows for tight integration of the DAE with the target, thereby increasing the chances for photomodulation of target functions. Nineteen different DAEs were synthesized and their properties investigated. All showed photochromism. Electron-withdrawing groups, and in particular –M-substituents at the triazole and/or thiophene moiety resulted in DAEs with high photo- and thermostability. Further, the chemical nature of the cyclopentene bridge had a strong influence on the behaviour upon UV light irradiation. Incorporation of perfluorinated cyclopentene led to compounds with high photo- and thermostability, but the reversible photochromic reaction was restricted to halogenated solvents. Compounds containing the perhydrogenated cyclopentene bridge, on the other hand, allowed the reversible photochromic reaction in a wide range of solvents, but had on average lower photo- and thermostabilities. The combination of the perhydrocyclopentene bridge and electron-withdrawing groups resulted in a DAE with improved photostability and no solvent restriction. Quantum chemical calculations helped to identify the photoproducts formed in halogenated as well as non-halogenated solvents. For two optimized DAE photoswitches, photostationary state composition and reaction quantum yields were determined. These data revealed efficient photochemical ring closure and opening. We envision applications of these new photochromic diarylethenes in photonics, nanotechnology, photobiology, photopharmacology and materials science.

Received 6th May 2021
Accepted 27th July 2021

DOI: 10.1039/d1sc02526k

rsc.li/chemical-science

Introduction

Diarylethenes (DAEs) are among the most commonly used classes of photochromic compounds. These molecules undergo a light-induced reversible electrocyclic ring closure reaction (Fig. 1(a)) which has little effect on end-to-end distance and dipole moment, but dramatically changes electronic properties, rigidity and rotational degrees of freedom. Since their first description in the late 1960s, literally thousands of DAE derivatives have been synthesized, characterized, and applied in many fields.[1] In addition to their originally intended application in optical information storage materials, DAEs have been incorporated into biomolecules,[2] molecular machines,[3–5] crystals,[6] surfaces[7] and nanoparticles,[8–10] as the reversible induction of structural changes by light promises attractive options for the modulation of chemical, physical, or biological properties. The incorporation of DAEs into target molecules typically requires multi-step organic synthesis, thereby limiting the application of these compounds. Often it would be desirable to attach a DAE to a pre-existing target structure – an organic molecule, a biopolymer, a 3D-nanotechnology object, a functional surface, or a macroscopic object. Ideally this would be possible in a fully site-specific manner, and orthogonal to the functional groups present in the target.

Examples for this approach are based on activated esters,[14,15] acetylenes,[12,13] carboxylic acids, and hydrazides,[16,17] but in these cases the DAE is typically appended to the target *via* linkers on the periphery of the photochromic unit. This connectivity provides flexibility and distance to the chromophore, which in turn attenuates or even eliminates the potential effects of DAE switching on the target's function.[8–10,15] A "zero-length"-linker

[a]*Institute of Pharmacy and Molecular Biotechnology (IPMB), Heidelberg University, Im Neuenheimer Feld 364, 69120 Heidelberg, Germany. E-mail: jaeschke@uni-hd.de*

[b]*Theoretical and Computational Chemistry, Interdisciplinary Center for Scientific Computing (IWR), Heidelberg University, Im Neuenheimer Feld 205A, 69120 Heidelberg, Germany*

† Electronic supplementary information (ESI) available: Supplementary figures, schemes and tables, experimental procedures, NMR spectra, computational details. See DOI: 10.1039/d1sc02526k

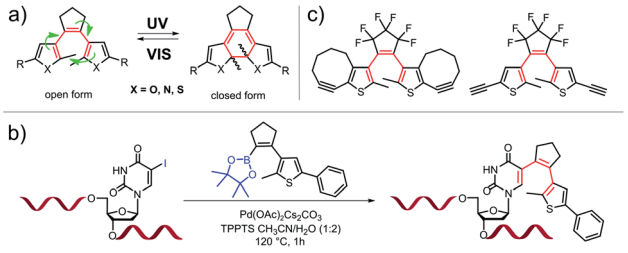

Fig. 1 Examples of known DAEs: (a) classical symmetric DAE structure and its reversible cyclization upon UV light irradiation (*R*: *e.g.* phenyl, OF: open form, CF: closed form), (b) "zero-length" linker synthesis of oligonucleotide-DAE photoswitches,[11] (c) examples of alkyne-substituted dithienyl-ethenes.[12,13]

would be more suitable for the tight integration of the DAE into the target's overall architecture. In a previous approach from our laboratory,[11] a precursor was synthesized that allowed the formation of a DAE in pre-assembled DNA strands by late-stage Suzuki–Miyaura cross coupling. A site-specifically placed iodo-substituent on a nucleobase was used to create a photoswitch where this nucleobase acted as one of the two aryl residues of the DAE (Fig. 1(b)). The approach of tight integration by late-stage zero-length linking should be amenable to considerable expansion. Theoretically, the various types of "click" chemistry[18] developed over the past two decades appear perfectly suited for such tight integration, and in particular those that involve azides, as various approaches for their site-specific incorporation have been developed (and in part commercialized) for biopolymers,[19] cyclodextrins,[20] nanoparticles,[21,22] surfaces,[23,24] and even some complex natural products.[25,26] While there are examples of attaching DAEs to targets by azide–alkyne based click chemistry, these again attach them to the periphery of the chromophore or *via* flexible linkers[12,13] (Fig. 1(c)). We are not aware of a single example where one of the DAE aryl rings is actually formed in a click reaction with a functional group of the target.

Here we report a new class of DAEs, in which one of the aryl rings is a 1,2,3-triazole. Importantly, this ring is formed in one step by copper-catalyzed alkyne–azide cycloaddition (CuAAC) using an azide group on the target and an alkyne that contains the DAE's bridge and another aryl ring (Fig. 2).

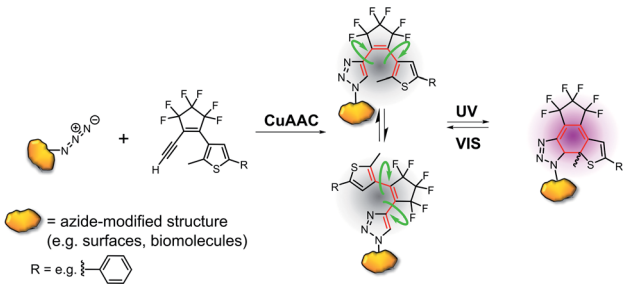

Fig. 2 Novel triazole DAE system: click reaction between an azide-modified target and a photoswitch precursor (cyclopentene-acetylene) forms a triazole diarylethene that is switchable between the flexible open and the rigid closed isomer, *R*: *e.g.* –phenyl.

We report the synthesis of 19 new DAEs, their analysis, and the optimization of their properties for applications as photoswitches. Our approach paves the way for the easy introduction of DAE photochromic units at strategically chosen positions of the target with zero-length connectivity and may facilitate applications in nanotechnology, photobiology, photopharmacology and materials science. By incorporating additional functional groups into the alkyne component, the approach can be easily expanded to allow the attachment of further building blocks (Fig. S1†).

Results and discussion

Design and synthesis of the alkyne component

At the outset of this study, it was unknown which structural features would render triazolyl-DAEs photochromic, reversible, fatigue-resistant, photo- and thermostable. To limit the combinatorial explosion of DAE diversity, we restricted ourselves to the following design features (Fig. 2): while one aryl of the DAE is represented by the triazole formed in the CuAAC, the second aryl should be a member of a small library of substituted 2-methylthiophenes, by far the most common aryl moiety in DAEs. With respect to the bridge moieties, we decided to stick with the two classical and most common ones, namely perfluorocyclopentene and cyclopentene (or perhydrocyclopentene). Thus, the first task at hand was to develop a synthetic route towards the alkyne component which consists of three elements: (i) the acetylene for the CuAAC reaction, (ii) the cyclopentene bridge, and (iii) the thiophene ring where limited diversity is introduced by further substitution (Fig. 2).

Coupling of acetylene groups to a perhydrocyclopentene ring has been reported, but the symmetrical 1,2-diacetylene-cyclopentene was unstable and turned brownish-black within minutes at room temperature.[27] For the synthesis of asymmetric cyclopentene acetylenes we adapted common synthesis routes for asymmetric diarylethenes by the introduction of an acetylene instead of the second aryl.

The synthesis of perfluorocyclopentene-bridged alkynes **6a–d** proceeded *via* compounds **5a–d** which are known intermediates in the synthesis of asymmetric DAEs[28–30] (Scheme 1(a)).

Trimethylsilyl-acetylene (TMS-acetylene) was introduced by lithiation analogous to the common introduction of the aryl moieties in high yields. The TMS protecting group was cleaved *in situ*, due to the release of fluorine ions in the coupling step, without compromising product formation. Compound **6d** was synthetized at lower temperatures (−90 °C (ref. 31)) to introduce the *tert*-butyl ester group.

Synthesis of perhydrocyclopentene acetylenes **9a** and **9b** was more challenging since acetylene coupling *via* Li–F-exchange reaction was not applicable. In the synthesis of DAEs of this type, the second aryl moiety is usually attached to the bridge by cross-coupling.[32,33] Sonogashira, Negishi and Stille conditions all gave the desired products, with the Stille coupling of (trimethylsilylethynyl)-tributylstannane (Scheme 1(b)) giving the highest yields and purities.

In contrast to the reported diacetylene cyclopentenes,[27] the acetylene-thienyl-cyclopentenes **6a–d** and **9a–b** showed

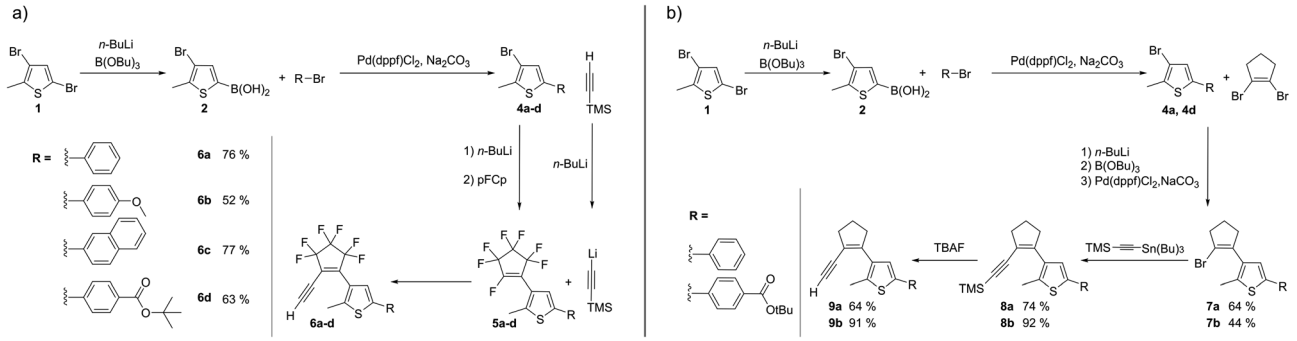

Scheme 1 (a) Synthesis of perfluorocyclopentene acetylenes **6a–d**. (b) Synthesis of perhydrocyclopentene acetylenes **9a** and **9b**.

sufficient stability for application in click reactions (see below). Perhydrocyclopentenes **9a–b** should be stored at −20 °C, as they turned brownish after a few days at room temperature. The perfluorinated derivatives **6a–d** were stable for months at room temperature, if undissolved and protected from light.

CuAAC synthesis of perfluorocyclopentene triazole photoswitches

The click reaction of the cyclopentene acetylene precursors was first investigated with perfluorocyclopentene acetylenes (**6a–d**) and small organic azides (**10a–l**). The lipophilic nature of the acetylenes required unpolar conditions, and the reaction was catalyzed by the [(1,10-phenanthroline)bis(triphenylphosphine)] copper(I)-nitrate dichloromethane adduct and additional copper(I) iodide (Scheme 2) at room temperature. This catalyst had been used even in solvent-free reactions[34] and turned out to be – in combination with copper(I) iodide – very efficient in the conversion of our new acetylenes in THF. 15 different triazole photoswitch derivatives (**pF$_{PS}$ 1–15**, abbreviation for **p**er**F**luorocyclopentene-**P**hoto**S**witch) were synthetized and characterized in order to derive first structure–property relationships for this novel DAE class, and to understand the effects of the reactant structure on the CuAAC reaction. In the first series, we kept the thiophene substituent R^2 constant and varied the azide substituent R^1 (for R^2 = phenyl: **pF$_{PS}$ 1–10**), while in a second series R^1 was kept constant (benzyl) and R^2 was varied (**pF$_{PS}$ 11–13**). A third set focused on the influence of R^1 and R^2 substituents with mesomeric effects (**pF$_{PS}$ 13–15**).

CuAAC allowed the synthesis of photoswitches from aromatic and aliphatic (including benzylic) azides, whereby the latter ones were obtained in higher yields. In most cases the conversion was complete after 1–3 hours, and stirring overnight did not induce significant side reactions. The phenyl thiophene-derivatized alkyne generally gave higher yields than the *p*-benzoic acid *tert*-butyl ester thiophene building block, and the combination of the latter with an electron-donating *N*,*N*-dimethylaminophenyl substituent was particularly low-yielding. Nevertheless, all target compounds could be synthesized by CuAAC.

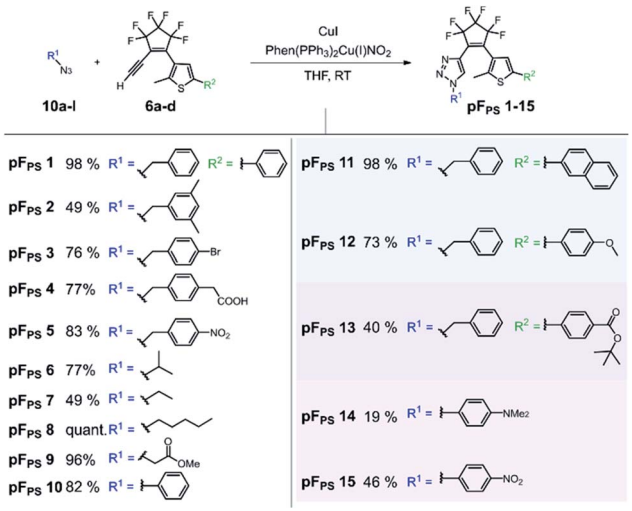

Scheme 2 CuAAC reaction yields of perfluorocyclopentene acetylene precursors (**6a–d**) with small organic azides (**10a–l**). 15 different triazole photoswitches were synthesized (**pF$_{PS}$ 1–15**).

Photochromism of pF$_{PS}$ 1

Upon irradiation with UV light at 254 nm or 310 nm, at different concentrations, light intensities and irradiation times, solutions of the first triazole photoswitch **pF$_{PS}$ 1** showed no significant photochromism in a range of commonly used non-halogenated solvents (methanol, ethyl acetate, dioxane or DMSO); they either retained their slightly brownish color, or their color changed irreversibly to faint yellow. However, solutions in halogenated solvents ($CHCl_3$, CH_2Cl_2, CH_2Br_2, and CCl_4) turned deeply red immediately, within seconds of UV light exposure.

Absorption spectroscopy revealed the formation of a new absorption band in the visible range upon UV irradiation, as is typical for DAEs (Fig. 3). Upon white-light illumination, the red color disappeared, indicative of the electrocyclic ring opening.

The process was found to be highly reversible, and the colored closed-ring form showed high photo- and thermostability ($\tau_{20\,°C}$ = 16.0 h in $CHCl_3$), indicating that this first triazolyl DAE performed very well, at least in halogenated solvents. We therefore characterized all 15 pF switches in $CHCl_3$, in order to obtain a basic understanding of the relationships between structure and switching properties. Concurrently, we attempted

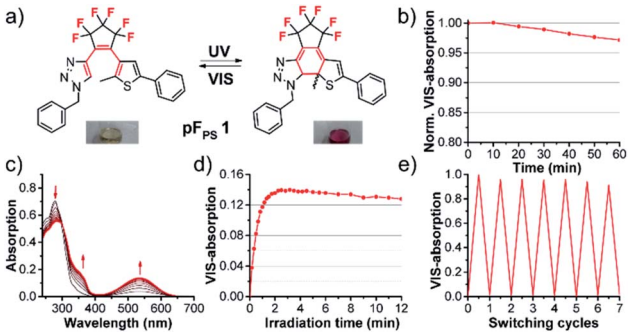

Fig. 3 Photochromism of pF$_{PS}$ 1 (60 μM solution in $CHCl_3$, irradiation at 310 nm, LED): (a) reversible electrocyclic ring closure, insets: photo of vial with colored solution, (b) thermostability of the closed form, monitored for 1 h at 20 °C at the VIS absorption maximum (534 nm), (c) evolution of the absorption spectra upon UV irradiation from the open form (black) towards the (pseudo-)photostationary state (p)PSS (red), (d) kinetic trace of the absorbance at 534 nm (VIS absorption maximum of the closed isomer) during prolonged UV irradiation, (e) reversibility measurement by alternating 310 nm and white-light illumination.

to design a structure that may allow a photochromic reaction in a wider range of solvents.

Understanding the role of the triazole substituents

Ten derivatives were analyzed that differed only in the triazole substituent (**pF$_{PS}$ 1–10**, Fig. 4). All compounds exhibited photochromism in chloroform, and among the alkyl-substituted compounds there was only little variation in the wavelength of the VIS absorption maximum (between 528 nm, **pF$_{PS}$ 9**, and 535 nm, **pF$_{PS}$ 2**, Fig. S2†), and the apparent extinction coefficient in the (pseudo)-photostationary state ((p)PSS, $\varepsilon_{VISmax,\,app}$, between 0.18×10^4 L (mol cm)$^{-1}$ (**pF$_{PS}$ 6**) and 0.40×10^4 L (mol cm)$^{-1}$ (**pF$_{PS}$ 9**), Fig. S2†). The bleaching behavior (*e.g.*, the absorbance *vs.* time trace after reaching the (p)PSS) showed slight differences, with compound **pF$_{PS}$ 2** being the most and compound **pF$_{PS}$ 4** the least photostable one. The largest differences were measured for the thermal stability of the closed-ring form (CF). Here, **pF$_{PS}$ 9** was the most and **pF$_{PS}$ 4**, again, the least stable one (Table S1†). This low performance of **pF$_{PS}$ 4** may be a consequence of the interaction between the acidic proton and the triazole ring. Attachment of an aromatic residue (**pF$_{PS}$ 10**) caused a large bathochromic shift of the VIS absorption band to 558 nm, an $\varepsilon_{VISmax,\,app}$ of 0.32×10^4 L (mol cm)$^{-1}$, and good (but not excellent) bleaching resistance and thermal stability. These observations correlate well with the structural diversity of the DAEs. Most obvious is the similarity of absorption *vs.* time traces within the group of benzyl derivatives, and the higher diversity of the traces among the derivatives with larger structural differences. Among the non-benzylic substituents, **pF$_{PS}$ 9** shows an exceptionally high thermostability, which may be caused by the electron withdrawing ester group in proximity to the triazole.

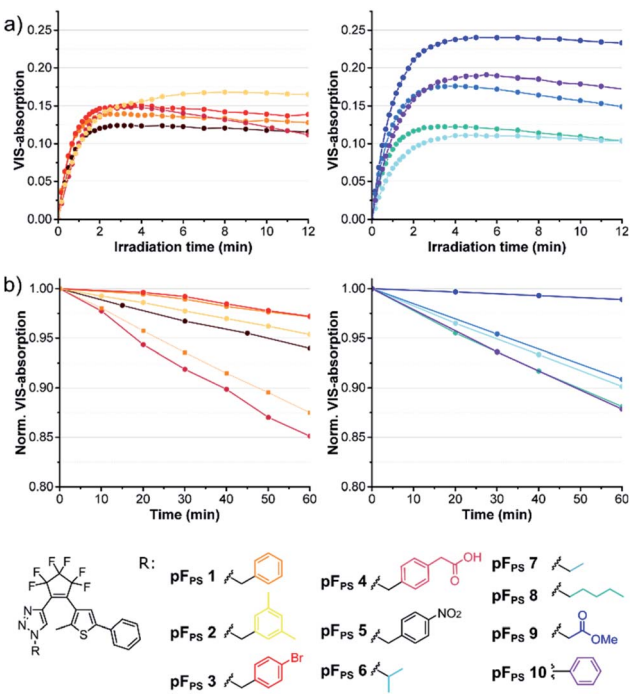

Fig. 4 Comparison of the photochromic properties of various alkyl triazole photoswitches pF$_{PS}$ 1–10 (60 μM solutions in chloroform): (a) kinetic trace of the absorbance at the VIS maximum, (b) thermostability (20 °C) of the closed-ring forms.

Role of the thiophene substitution

Comparing **pF$_{PS}$ 1** and **pF$_{PS}$ 13** (Fig. 5) with each other revealed the effects of adding an ester group to the *p*-position of the phenyl ring: increased absorption of the open form (OF), small bathochromic shift of the (p)PSS maximum (2 nm), increased (p)PSS absorption (from 0.14 to 0.23), similar photostability, and only slightly reduced thermostability. If an electron-donating methoxy group was added instead of the electron-withdrawing ester (**pF$_{PS}$ 12**), λ_{max} was bathochromically shifted by 11 nm, $\varepsilon_{VISmax,\,app}$ was increased to 0.47×10^4 L (mol cm)$^{-1}$), and a very high thermal stability ($\tau_{20\,°C} = 21.2$ h) was observed (Fig. 5). In addition, the spectral differences between open and closed form of this switch were particularly large. On the other hand, photostability was significantly reduced for this electron-rich photochrome. A similar trend was seen when the π-system of **pF$_{PS}$ 1** was extended from phenyl to naphthyl (**pF$_{PS}$ 11**).

Thus, the substituents at the thiophene ring exert a much stronger influence on the photochromic properties than those on the triazole ring described above (Fig. 4).

Structure optimization using mesomeric effects

During the systematic variation of the triazole substituents (Fig. 4) we observed that the change from alkyl to aryl substituents has a strikingly large influence on the VIS absorption wavelength of the closed isomers (see also Fig. S2†). This behavior indicates that the conjugation of the phenyl ring extends into the chromophore of the closed ring form, and implies that +M or −M substituents attached to the phenyl ring might efficiently modulate the properties of these DAEs. We tested this hypothesis using compounds with benzoic acid *tert*-butylester as the thiophene substituent. The rationale behind

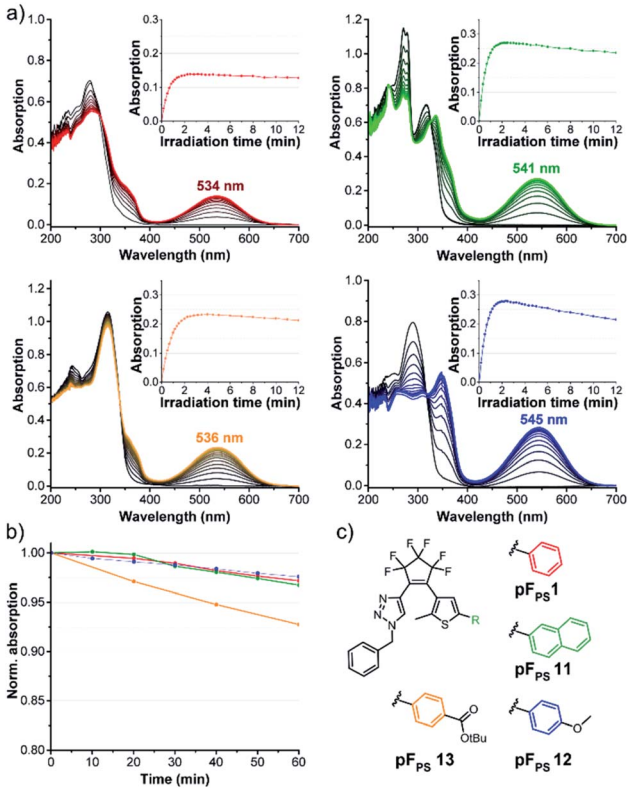

Fig. 5 Photochromic properties of various thienyl substitutions: (a) time-dependent changes of the absorption spectra of 60 μM solutions of **pF$_{PS}$ 1**, **11–13** upon UV light irradiation (310 nm, LED) in chloroform towards the (pseudo)-photostationary state; insets show the absorption *vs.* time trace measured at the VIS absorption maximum during extended UV irradiation to analyse the photostability, (b) thermostability (20 °C) of the CF isomers, (c) structures.

this choice was the option to later use the ester function for further late-stage functionalization or cross-linking, *e.g.*, by amide coupling. We furthermore expected the ester to lead to higher photostabilities, compared to an +M substituent (compare **pF$_{PS}$ 13** and **pF$_{PS}$ 12**, Fig. 5). We directly compared an electron-withdrawing aromatic *para*-nitrophenyl substituent (**pF$_{PS}$ 15**) with an electron-donating aromatic *para*-*N*,*N*-dimethylaminophenyl (**pF$_{PS}$ 14**) and a benzyl substituent (**pF$_{PS}$ 13**) at the triazole (Fig. 6). Again, all compounds were photochromic. **pF$_{PS}$ 14** showed broad absorption features (with two maxima), low $\varepsilon_{VISmax,\ app}$ (0.18×10^4 L (mol cm)$^{-1}$), strong bleaching and low thermal stability. Overall, these results indicated that increased electron density at the triazole ring (+M effect) results in decrease photo- and thermostability. For **pF$_{PS}$ 15**, a very strong band ($\varepsilon_{VISmax,\ app} = 0.53 \times 10^4$ L (mol cm)$^{-1}$) with a strongly bathochromically shifted maximum at 565 nm, high thermo- and photostability was observed. Thus, the combination of two aromatic −M substituents R^1 and R^2, as in **pF$_{PS}$ 15**, creates particularly performant photoswitches, at least in halogenated solvents.

However, none of the 15 pF compounds showed reversible photochromism in non-halogenated solvents. Overall, the addition of functional groups to a phenyl substituent has much stronger overall influence on the photochromic properties on the triazole side, compared to the thiophenyl side (Table S1†). In summary, **pF$_{PS}$ 15** can be considered an optimized structure among the pF-photoswitches.

Synthesis and photochromism of perhydrocyclopentene photoswitch pH$_{PS}$ 1

To investigate the influence of the bridge moiety on the properties of triazolyl-DAEs, we converted perhydrocyclopentene acetylenes **9a**and **9b** under the same CuAAC reaction conditions in yields similar to those of the pF-switches (see details in Scheme S1†). Next, we characterized benzyl-phenyl compound **pH$_{PS}$ 1** and compared its properties to its sister compound **pF$_{PS}$ 1** (Fig. 7).

For **pH$_{PS}$ 1**, the VIS absorption band formed upon UV irradiation in chloroform was hypsochromically shifted by 47 nm,

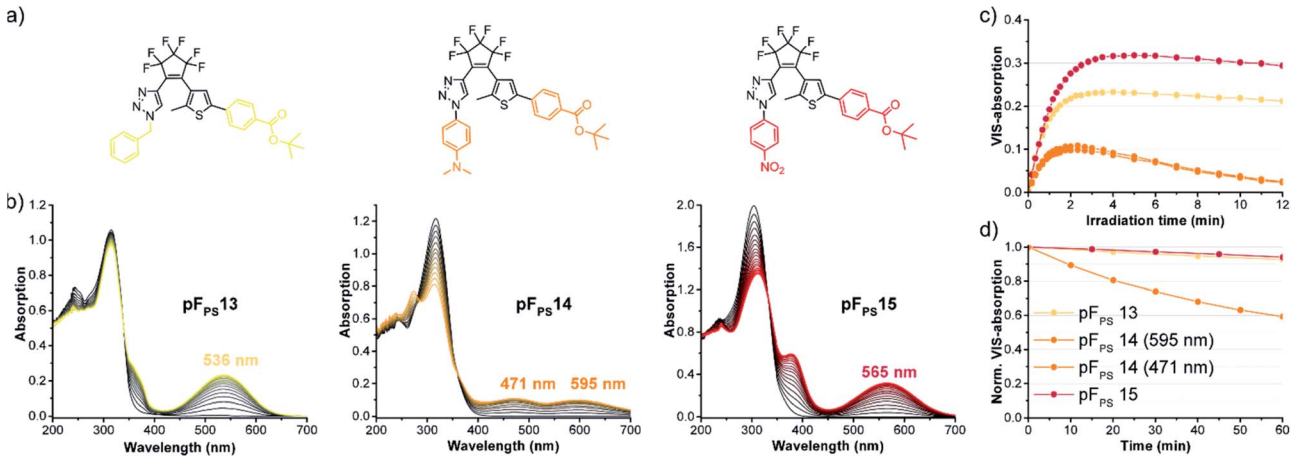

Fig. 6 Effect of electron-donating and electron-withdrawing substituents at the triazole ring on the photochromic properties: (a) structures of **pF$_{PS}$ 13–15**, (b) time-dependent changes of the absorption spectra of solutions (60 μM in $CHCl_3$) during UV light irradiation (310 nm UV light) to the (pseudo)-photostationary state, (c) kinetic trace of the VIS absorption bands during extended UV irradiation, (d) thermostability (20 °C) of the CF isomers.

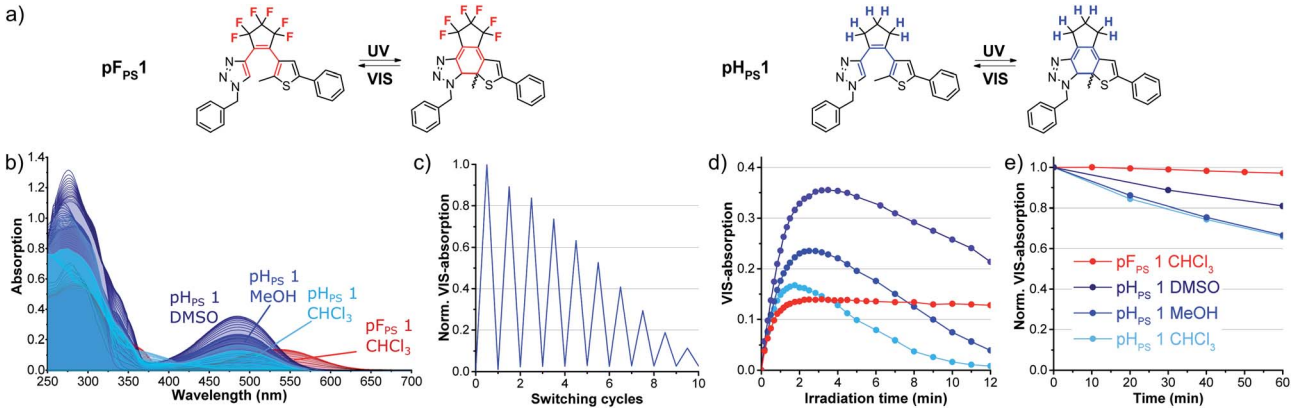

Fig. 7 Comparison of triazole photoswitches with perfluorinated (**pF$_{PS}$ 1**) and perhydrogenated (**pH$_{PS}$ 1**) cyclopentene bridge: (a) structures of the respective OF and CF isomers, (b) time-dependent changes in the absorption spectra upon UV light irradiation in different solvents (310 nm, 60 μM conc.) to the (p)PSS, (c) reversibility of **pH$_{PS}$ 1** in methanol, (d) kinetic trace of the VIS absorption bands (CF isomers) during extended UV light irradiation, (e) thermostability (20 °C), see also Table S4.†

compared to the band of the perfluorinated analog **pF$_{PS}$ 1** (Fig. 7(b)). The switching process was found to be reversible, although a high photobleaching rate led to a fast decrease of the VIS absorption over 10 reaction cycles (Fig. 7(c)). The low photostability was also detected in the kinetic trace of the VIS absorption during extended UV irradiation (Fig. 7(d)). Advantageously, however, **pH$_{PS}$ 1** showed photochromism not only in halogenated solvents, but also in methanol and DMSO. The VIS absorption bands formed in these solvents appeared at exactly the same wavelengths as in chloroform. The highest $\varepsilon_{\mathrm{VISmax,\ app}}$ was measured in DMSO (0.60×10^4 L (mol cm)$^{-1}$), however the bleaching rate was high in all three tested solvents. For **pH$_{PS}$ 1**, chloroform was inferior to the other solvents with respect to $\varepsilon_{\mathrm{VISmax,\ app}}$ and bleaching. The highest thermal stability of the closed-ring form was measured in DMSO, too (80% remaining after 1 h, $\tau = 2.6$ h, 20 °C). Overall, with the exception of $\varepsilon_{\mathrm{VISmax,\ app}}$, perhydrocyclopentene switch **pH$_{PS}$ 1** was inferior to its perfluorinated sister compound (Fig. 7(c–e)). The electronegative fluorine atoms had a positive effect on photo- and thermostability. Nevertheless, the perfluorocyclopentene bridge caused an incompatibility with most solvents, while perhydrocyclopentene was found to overcome this solvent restriction.

Investigation of the irreversible reaction of pFPS 1 in non-halogenated solvents

While solvent-dependent photochromism of DAEs is known,[35–37] the selective photochromism in halogenated solvents only, as observed for all our perfluorocyclopentene diarylethenes, had not been described before (to our knowledge). We therefore investigated the photochromism of compound **pF$_{PS}$ 1** in a wider panel of solvents.

When irradiated in methanol, DMSO, ethyl acetate, or dioxane, **pF$_{PS}$ 1** formed a new intense absorption band outside the visible spectrum (Fig. S3,† blue spectra). The formation of this absorption band ($\lambda_{max} = 420$ nm in DMSO, ~372 ± 1 nm in all other solvents) was irreversible: neither irradiation with a white-light lamp nor with LEDs emitting near this maximum had any effect on the absorption spectrum of the solution. Furthermore, no bleaching was observed during extended 310 nm illumination. Analysis of the absorption *vs.* time traces (at 373 nm, the newly formed maximum during the irradiation) in DMSO revealed a sigmoidal course in the early phase of the reaction (Fig. 8). This observation may indicate a fast consecutive reaction that consumes the initially formed CF isomer.[1,38] Indeed, in DMSO the intermittent formation of CF was revealed by the $A_{510\mathrm{nm}}$ *vs.* time trace that quickly ($t < 1$ min) reached a maximal value and then declined, while the inflection point of the curve at $A_{373\mathrm{nm}}$ correlated exactly with the maximum of $A_{510\mathrm{nm}}$ (Fig. S4a†). In methanol, the rate of the consecutive reaction was much higher than in DMSO, the concentration of CF remained very low, and the initial slope of the curve was much steeper (Fig. 8).

On the other hand, in dibromomethane the side reaction was slowed down considerably, so that both processes (the formation of the VIS absorption bands of the closed form and the UV-band of the byproduct) could be well observed on the

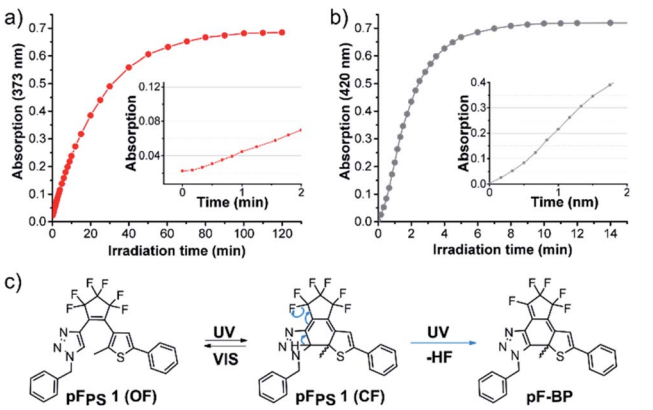

Fig. 8 Kinetic trace of absorption bands formed in **pF$_{PS}$ 1** solutions during UV light irradiation (310 nm, 60 μM in (a) methanol (absorption band at 373 nm) and (b) DMSO (absorption band at 420 nm), (c) hypothetic reactions of **pF$_{PS}$ 1** in these solvents and the assumed structure of the specific side product **pF-BP**.

same time scale (Fig. S4c†). Samples taken during irradiation of a methanolic solution of **pF_{PS} 1** were analyzed by HPLC (Fig. S5†). Concurrent to the decrease of the peak of the OF isomer (12.9 min retention time), a new peak appears at 14.3 min that absorbs strongly at 373 nm, suggesting that only one product is formed in significant amounts. This product was isolated by column chromatography (ESI, chapter 2.2.5†) to obtain a yellow solid with a mass (508.0879 *m*/*z* (M + Na)) 20 *m*/*z* units smaller than the mass of **pF_{PS} 1**(528.0932 *m*/*z* (M + Na)). ^{1}H-NMR spectra indicated diastereotopic CH_2-protons and the ^{19}F-spectrum revealed a pattern of nine distinct fluorine signals (Fig. S6†), both findings suggesting the elimination of HF, as observed for the CF of DAEs by others.[39–41] The electronic structure of the closed triazole photoswitches could favor HF-elimination, as the high electronegativity of the six fluorine and three nitrogen atoms should acidify the triazole proton, leading to the reaction product proposed in Fig. 8(c) and S7.† Products of the often-described annulation (formally by a 1,2-dyotropic rearrangement)[1,38,42,43] and the HF elimination would still have an extended π-system with a fulvene-like structure which can be expected to be strongly colored, too,[44] which is not the case for our isolated side product. Considering additionally the energetically favorable restoration of the aromatic triazole, and the small difference in the chemical shifts of the CH_2-protons between **pF_{PS} 1** and the bleaching product, the elimination from the closed isomer is – in our opinion – the more likely process.

HPLC analysis of the UV-induced photocyclization of perhydro sister compound **pH_{PS} 1** revealed the formation of a peak eluting at 15.1 min with strong absorption at 486 nm, indicative of the closed isomer (Fig. S5†), while no signal of a specific rearrangement product was observed. After reaching the (p)PSS, the absorption decreases over a wide wavelength range (>250 nm), suggestive of unspecific bleaching.

Thus, the cyclopentene bridge has a strong influence on the photochromic properties of the triazole photoswitches, and it also determines the scope of solvents that can be used in the desired application. Why the HF elimination is prevented in halogenated solvents is not clear at this point. A coordination effect between the solvent and the triazole ring is conceivable as well as energetic effects by solvation, raising the possibility to modulate this aspect by structural modifications at the triazole ring. In conclusion, an important design consideration for photochromism that is not limited to chlorinated solvents is the use of cyclopentene bridges that do not allow 1,4-elimination reactions.

Computational investigation of the photoswitching mechanism of pF_{ps} 1

The photochemical switching mechanism underlying the photochromism of DAEs has been investigated previously, in particular for derivatives with two thiophene rings as aryl moieties.[1,45–47] The switching mechanism has been shown to proceed efficiently *via* a conical intersection.[48–50] In the DAEs synthesized here, one of the thiophene rings is replaced by triazole with substantially different molecular properties, and the first question to address is thus whether this has an influence on the switching mechanism.

Among our different perfluorocyclopentenyl photoswitches, **pF_{PS} 1** was taken as representative for further quantum chemical investigation at standard time-dependent density functional theory (DFT)[51,52] level using ωB97X-D[53] as the exchange–correlation functional and cc-pVDZ basis set. The conductor-like polarizable continuum model (CPCM)[54] was used to incorporate bulk solvent effects. Since the open-form of **pF_{PS} 1** is highly flexible, among other stable isomers (Table S2†), most possess an outward skewed geometry with the $-CH_3$ group on the thiophene sticking out of the molecular plane (see Fig. 9, **pF_{PS} 1**(OF)). The terminal C–C separation along the reaction coordinate in this geometry is 3.4 Å, and this geometry has been chosen for our calculation of the vertical excited states of **pF_{PS} 1**.

To investigate the light-induced ring closure mechanism upon vertical excitation of the OF ground state to the first excited S_1 state, a relaxed scan of the S_1 potential energy surface has been performed along the C–C distance formed during ring closure (Fig. 10). According to our calculations, the reactive first excited state of both conformers corresponds essentially entirely to the HOMO–LUMO transition. The frontier orbitals are shown in Fig. 9. Since a conical intersection is expected to be involved in the reaction, spin-flip-TDDFT[55] has been used for this calculation. As can be seen in Fig. 10, a conical intersection is present at a C–C distance of 2.1 Å. Hence, upon vertical excitation of the OF, the molecules undergo a barrierless ring-closure reaction towards the conical intersection, at which they can switch efficiently into the closed-form electronic ground state. The C–C bond length of the newly formed bond is found to be 1.53 Å. Thus, our analysis revealed that **pF_{PS} 1** indeed undergoes an electrocyclic ring closure through a conical intersection in analogy to other DAEs,[48–50] indicating that the introduction of a triazole ring in the DAE does not disturb their common photoswitching mechanism.

The $-CH_2$ group in the benzyl substituent on the triazole ring breaks the extended π-conjugation which exists throughout the structure. Furthermore, it can be seen that there is no

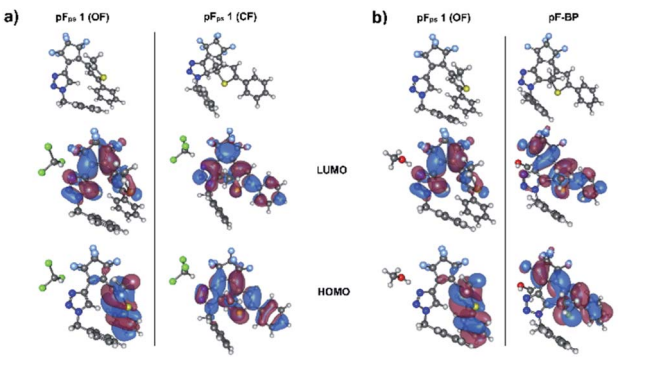

Fig. 9 Frontier MOs: HOMO and LUMO from wB97X-D/cc-pvdz/PCM full TDDFT calculations for the two different solvents. (a) OF and CF in $CHCl_3$ (b) OF and BP in MeOH.

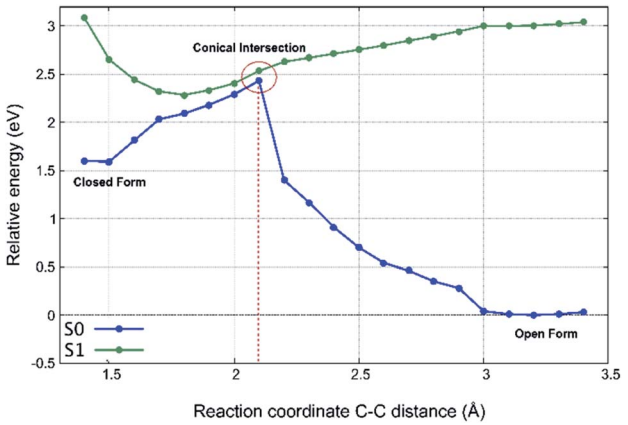

Fig. 10 Potential energy scan for the first excited state (S1) and the ground state (S0) along relaxed S1 geometries along the reaction coordinate. The intersection denotes the approximate crossing point of the surfaces.

contribution from the benzyl fragment to the frontier orbitals (Fig. 9). As a result, the first singlet electronic transition remains unaffected from the presence of the benzyl substituent. This phenomenon can also be observed in the other derivatives where the π-conjugation is hindered due to a $-CH_2$ bridge (**pF_{PS} 1–5**, Fig. 4). Derivatives with an extended conjugation, on the other hand, show markedly different spectra of the CFs in halogenated solvents (**pF_{PS} 14** and **pF_{PS} 15** with phenyl substituents).

Identification of the irreversible intermediate in non-halogenated solvents

pF_{PS} 1 and the other perfluorinated derivatives exhibit an entirely different behavior in halogenated *vs.* non-halogenated solvents (see Fig. S3†). To model the effect of the $CHCl_3$ solvent, the ground state geometries of the open and closed forms were coordinated with one $CHCl_3$ molecule (Fig. 9(a)), and their geometry re-optimized, followed by a full TD-DFT/ωB97x-D/cc-pvdz/PCM calculation for their corresponding absorption spectra (Fig. 11).

The absorption maximum for the OF of **pF_{ps} 1** is calculated to be at 276 nm, which is in excellent agreement with the experimental value of 280 nm. The absorption maximum of the CF is calculated to be at 489 nm, however, this peak is blue shifted by 28 nm (0.21 eV) relative to the measured value, which is the typical accuracy of the chosen methodology.[56,57] The same trends are found for the OF and CF of the parent **pH_{ps} 1**, which is shown in Table S3.†

In Fig. 11(a), the time-dependent changes in the absorption spectrum of the open form of **pF_{PS} 1** are modeled in chloroform assuming a quantitative conversion to the CF. Therefore, spectra of OF and CF are plotted together with 3 : 1, 1 : 1, and 1 : 3 superpositions thereof. Comparison with the corresponding experimental spectra demonstrates an excellent agreement, supporting the above-described photoswitching mechanism in halogenated solvents.

In non-halogenated solvents, for example MeOH, experimental evidence is given that irreversible elimination of HF takes place, thereby quenching the photoswitching reaction. To support this assumption, the time-dependent changes in the absorption spectra of **pF_{PS} 1** have been modeled following the same procedure as above, now with the elimination byproduct **pF-BP** (Fig. 9(b), for further structural details see Fig. S7†) as final state of the time evolution. The elimination extends the aromaticity to the perfluorocyclopentene ring due to increased π-conjugation. The simulated absorption maximum for the elimination product is at 345 nm (Fig. 11), which is slightly blue-shifted relative to the experimental value of 373 nm, well within the typical range of error of the method.[56,57]

Again, the agreement between the simulated and measured absorption spectra in CH_3OH is good, corroborating the

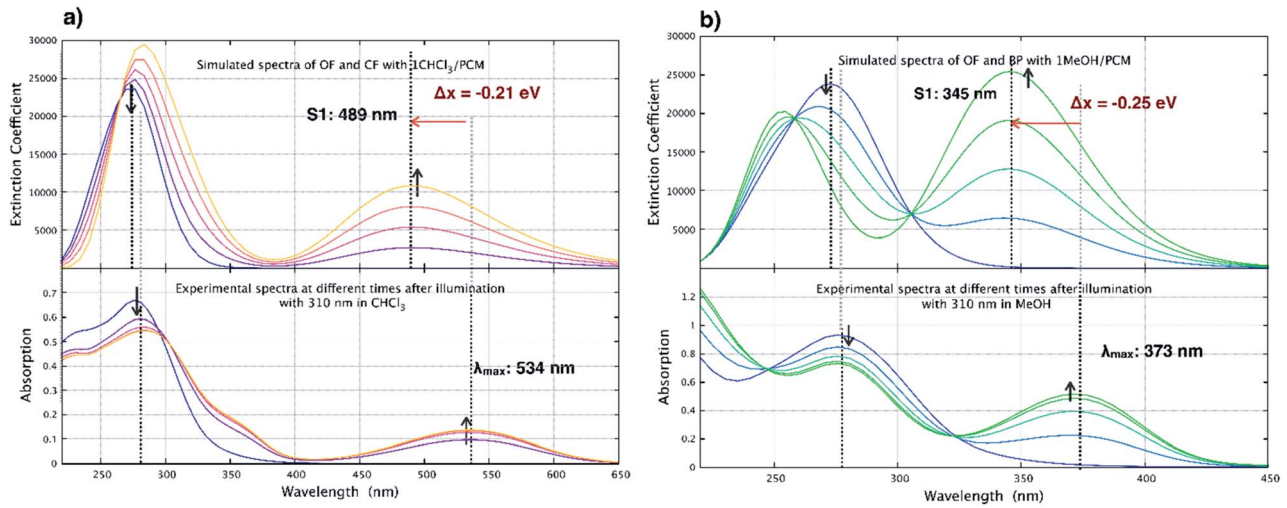

Fig. 11 Comparison between experimental spectra and simulated spectra in (a) $CHCl_3$ and (b) MeOH. The computational spectra are plotted for mixtures of OF and corresponding end product in varying ratios in the two solvents using wB97X-D/cc-pvdz/PCM for geometries in Fig. 10.

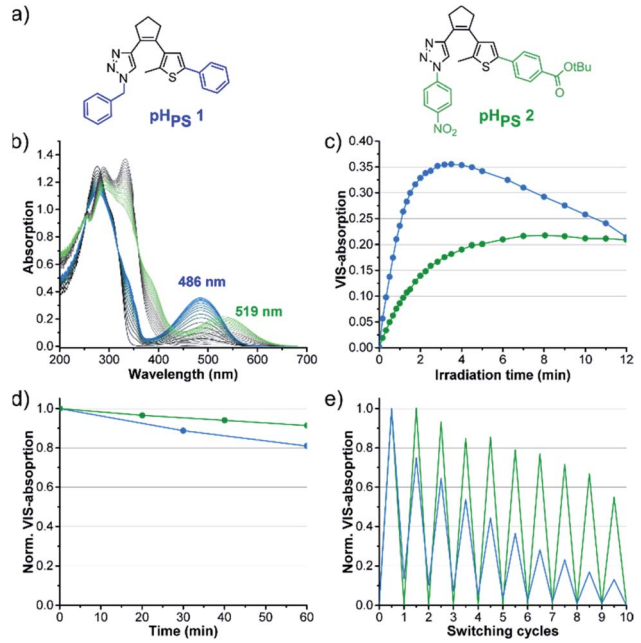

Fig. 12 Effect of structure optimization on the photochromic properties: (a) structures of pH_{PS} 1 and pH_{PS} 2, (b) absorption spectra change of 60 μM solutions of pH_{PS} 1 and pH_{PS} 2 during UV light irradiation (310 nm, LED) in DMSO to the (p)PSS, (c) kinetic trace of the VIS absorption bands during prolonged UV illumination, (d) thermostability (20 °C), (e) reversibility measurement (normalized VIS absorption).

elimination reaction to be the main reaction path in non-halogenated solvents.

The origin of this very unusual solvent dependency needs further theoretical modeling of the solute–solvent interactions that go beyond the current work. This will likely require extensive sampling of the solvent environment, the weak but explicit solute–solvent interactions, and possibly even the interaction with several solvent molecules, which altogether make such simulations extremely demanding, if they are currently possible at all.

Optimization of the triazole photoswitch structure

Further investigations with different derivatives of **pH_{PS} 1** revealed that among the perhydrocyclopentene triazole DAEs, the substituents have an even stronger influence on the photochromic properties than in the perfluorocyclopentene series (Fig. S8 and Table S4†). Thus, the structure of the pH photoswitches could be further optimized, applying the knowledge about the structure–property relationships obtained in the pF series. As −M substituents on both rings were found to be beneficial, we synthesized and characterized the perhydrocyclopentene analog of our optimized compound **pF_{PS} 15**, combining a *p*-nitrophenyl substituent on the triazole and *p*-benzoic acid *tert*-butyl ester on the thiophene ring. The resulting compound **pH_{PS} 2** (Fig. 12(a)) shows actually much higher photostability than **pH_{PS} 1**, retaining 96% of its maximal VIS absorption after 12 minutes of UV light irradiation in DMSO (Fig. 12(c) and Table S4†).

The thermostability was improved, too ($\tau_{20\ °C}$: 5.9 h *vs.* 2.6 h for **pH_{PS} 1**, Fig. 12(d), Table S4†), and a higher degree of reversibility could be reached (Fig. 12(e)). While the properties are still far from perfect, these data indicate the directions for further optimization, *e.g.*, by the addition of further electron-withdrawing groups on the triazole-phenyl ring.

Photostationary state composition and quantum yields

For most of the novel DAEs described here, the solvent dependence or restriction of photochromism in combination with the imperfect thermo- and photostability prevented an exact determination of (p)PSS composition and quantum yields. For our two optimized compounds, **pF_{PS} 15** and **pH_{PS} 2**, however, we could estimate these parameters. For the perhydrocyclopentene switch **pH_{PS} 2**, OF and CF of (p)PSS mixtures in DMSO were separated by reversed-phase HPLC and the composition determined from the integrated peak areas, taking into account decomposition during the analysis (Table 1 and Fig. S9†). The (p)PSS^{UV} was found to contain 58–60% CF, while the PSS^{Vis} contained ∼0% CF, as indicated by the reduction to zero of the 519 nm absorbance band upon vis light illumination (Fig. 12(e)). Ring closing and ring opening quantum yields were determined as reported previously[58,59] and indicate a rather efficient photochemistry. A most striking feature is the high quantum yield of ring opening upon irradiation with 505 nm visible light (0.56), which compares favorably with classical dithienylethenes where this value is often smaller than 0.01.

As perfluorocyclopentene switch **pF_{PS} 15** could not be analyzed by HPLC, we prepared 15 ml of a 100 μM solution in $CDCl_3$, irradiated to the PSS^{UV}, then quickly concentrated the reaction mixture *in vacuo*, and analyzed it by ^{1}H-NMR spectroscopy (Table 1 and Fig. S10†). This analysis revealed a PSS^{UV} composition of 55–58% CF, while the reversibility measurements (Fig. 3e) indicate a PSS^{Vis} content of ∼0% CF. The ring opening quantum yield (in $CHCl_3$) was slightly lower than for **pH_{PS} 2**.

Table 1 (p)PSS composition and quantum yields of pH_{PS} 2 and pF_{PS} 15

	$PSS^{UV a}$ [%]	$PSS^{Vis b}$ [%]	$\phi_{OC}{}^{UV c}$ [%]	$\phi_{OC}{}^{UV d}$ [%]	$\phi_{CO}{}^{Vis e}$ [%]	$\phi_{OC}/\phi_{CO}{}^{UV f}$
pH_{PS} 2	58–60	0	31	29	56	1.07
pF_{PS} 15	55–58	0	39	40	45	0.98

[a] Photostationary state after irradiation with UV light, in % CF. [b] Photostationary state after irradiation with Vis light, in % CF. [c] Ring cyclization quantum yields at 325 nm and 300 nm, respectively. [d] Ring opening quantum yields at 325 nm and 300 nm, respectively. [e] Ring cyclization quantum yields at 505 nm and 567 nm, respectively. [f] Ratio of ring closing to ring opening quantum yields upon UV irradiation.

Conclusions

A new class of DAEs was designed which allows the generation of the photochromic moiety by CuAAC in direct proximity to the attachment point, using azide groups present in the target structures. Several systematically varied DAEs were synthesized from small organic azides, and the structure–property relationships of the compounds were determined by absorption spectroscopy and DFT calculations. Based on this knowledge, a first structural optimization was carried out, and the optimized DAEs already had properties which may permit a wide range of applications. The high conversion in the photostationary states and the high reaction quantum yields make these novel DAEs particularly attractive for applications in photonics, where fast and efficient back-and-forth switching is desired.[60] However, there is still plenty of room for further structural modifications. Our next step will be the application of the acetylene precursors developed here for the modification of azido-derivatized amino acids and peptides.

Data availability

The data supporting the findings of this study are available within the paper and its ESI† files.

Author contributions

S. B. and A. J. conceived the project. S. B. designed, synthesized and characterized the compounds and analyzed the data. S. M. B. determined quantum yields and photostationary state compositions. R. S. and A. D. conducted the theoretical investigations and supported the elucidation of the structure of pF-BP. S. B. and A. J. wrote the initial draft of the manuscript. All authors contributed to the writing, editing and proof-reading process.

Conflicts of interest

There are no conflicts to declare.

Acknowledgements

This work was supported by the Federal Ministry of Education and Research (BMBF), grant # 031A170B. The authors gratefully acknowledge technical support by S. Suhm, T. Timmermann and H. Rudy. We furthermore thank A. H. Becker, S. Braun, B. Bühler, S. Feth, N. Kipper, F. S. Menke and L. Petersen for assistance in the synthesis. The computational work was conducted within the Collaborative Research Center "N-heteropolycycles as functional materials" (SFB1249) of the German Science Foundation. Reena Sen received financial support from the Heidelberg graduate school, "Mathematical and Computational Methods in the Sciences" (GSC 220).

References

1 M. Irie, T. Fulcaminato, K. Matsuda and S. Kobatake, *Chem. Rev.*, 2014, **114**, 12174–12277.
2 Z. L. Pianowski, *Chem.–Eur. J.*, 2019, **25**, 5128–5144.
3 S. Corra, M. Curcio, M. Baroncini, S. Silvi and A. Credi, *Adv. Mater.*, 2020, **32**, 1906064.
4 M. Q. Li, L. J. Chen, Y. S. Cai, Q. F. Luo, W. L. Li, H. B. Yang, H. Tian and W. H. Zhu, *Chem*, 2019, **5**, 634–648.
5 H. Zhang, X. X. Kou, Q. Zhang, D. H. Qu and H. Tian, *Org. Biomol. Chem.*, 2011, **9**, 4051–4056.
6 T. I. Lansakara, F. Tong, C. J. Bardeen and A. V. Tivanski, *Nano Lett.*, 2020, **20**, 6744–6749.
7 I. Hnid, D. Frath, F. Lafolet, X. N. Sun and J. C. Lacroix, *J. Am. Chem. Soc.*, 2020, **142**, 7732–7736.
8 H. Yamaguchi, M. Ikeda, K. Matsuda and A. Irie, *Bull. Chem. Soc. Jpn.*, 2006, **79**, 1413–1419.
9 T. Kudernac, S. J. van der Molen, B. J. van Wees and B. L. Feringa, *Chem. Commun.*, 2006, 3597–3599.
10 A. Ghavidast and N. O. Mahmoodi, *J. Mol. Liq.*, 2016, **216**, 552–564.
11 H. Cahova and A. Jäschke, *Angew. Chem., Int. Ed.*, 2013, **52**, 3186–3190.
12 A. V. Strizhak, K. Sharma, O. Babii, S. Afonin, A. S. Ulrich, I. V. Komarov and D. R. Spring, *Org. Biomol. Chem.*, 2018, **16**, 8559–8564.
13 F. Hu, M. Hu, W. J. Liu, J. Yin, G. A. Yu and S. H. Liu, *Tetrahedron Lett.*, 2015, **56**, 452–457.
14 K. Fujimoto, M. Kajino, I. Sakaguchi and M. Inouye, *Chem.–Eur. J.*, 2012, **18**, 9834–9840.
15 N. Soh, K. Yoshida, H. Nakajima, K. Nakano, T. Imato, T. Fukaminato and M. Irie, *Chem. Commun.*, 2007, 5206–5208.
16 O. Babii, S. Afonin, M. Berditsch, S. Reisser, P. K. Mykhailiuk, V. S. Kubyshkin, T. Steinbrecher, A. S. Ulrich and I. V. Komarov, *Angew. Chem., Int. Ed.*, 2014, **53**, 3392–3395.
17 K. Fujimoto, T. Maruyama, Y. Okada, T. Itou and M. Inouye, *Tetrahedron*, 2013, **69**, 6170–6175.
18 H. C. Kolb, M. G. Finn and K. B. Sharpless, *Angew. Chem., Int. Ed.*, 2001, **40**, 2004–2021.
19 M. Aigner, M. Hartl, K. Fauster, J. Steger, K. Bister and R. Micura, *Chembiochem*, 2011, **12**, 47–51.
20 M. Gerowska, L. Hall, J. Richardson, M. Shelbourne and T. Brown, *Tetrahedron*, 2012, **68**, 857–864.
21 L. H. Liu and M. D. Yan, *Acc. Chem. Res.*, 2010, **43**, 1434–1443.
22 J. Park, H. S. N. Jayawardena, X. Chen, K. W. Jayawardana, M. Sundhoro, E. Ada and M. D. Yan, *Chem. Commun.*, 2015, **51**, 2882–2885.
23 J. P. Collman, N. K. Devaraj and C. E. D. Chidsey, *Langmuir*, 2004, **20**, 1051–1053.
24 A. Devadoss and C. E. D. Chidsey, *J. Am. Chem. Soc.*, 2007, **129**, 5370–5371.
25 S. J. Luchansky, H. C. Hang, E. Saxon, J. R. Grunwell, C. Y. Danielle, D. H. Dube and C. R. Bertozzi, *Methods Enzymol.*, 2003, **362**, 249–272.
26 J. W. Chin, S. W. Santoro, A. B. Martin, D. S. King, L. Wang and P. G. Schultz, *J. Am. Chem. Soc.*, 2002, **124**, 9026–9027.
27 A. J. Ashe and F. J. Drone, *J. Am. Chem. Soc.*, 1987, **109**, 1879–1880.

28 A. Peters, C. Vitols, R. McDonald and N. R. Branda, *Org. Lett.*, 2003, **5**, 1183–1186.
29 S. Kobatake and M. Irie, *Tetrahedron*, 2003, **59**, 8359–8364.
30 F. Sun, F. H. Zhang, H. B. Guo, X. H. Zhou, R. J. Wang and F. Q. Zhao, *Tetrahedron*, 2003, **59**, 7615–7621.
31 W. E. Parham and L. D. Jones, *J. Org. Chem.*, 1976, **41**, 2704–2706.
32 M. Singer and A. Jäschke, *J. Am. Chem. Soc.*, 2010, **132**, 8372–8377.
33 T. C. Pijper, T. Kudernac, W. R. Browne and B. L. Feringa, *J. Phys. Chem. C*, 2013, **117**, 17623–17632.
34 D. Wang, M. M. Zhao, X. Liu, Y. X. Chen, N. Li and B. H. Chen, *Org. Biomol. Chem.*, 2012, **10**, 229–231.
35 V. Aubert, E. Ishow, F. Ibersiene, A. Boucekkine, J. A. G. Williams, L. Toupet, R. Metivier, K. Nakatani, V. Guerchais and H. Le Bozec, *New J. Chem.*, 2009, **33**, 1320–1323.
36 L. Ordronneau, J. Boixel, V. Aubert, M. S. Vidal, S. Moya, P. Aguirre, L. Toupet, J. A. Williams, H. Le Bozec and V. Guerchais, *Org. Biomol. Chem.*, 2014, **12**, 979–992.
37 H. Xi, Z. Zhang, W. Zhang, M. Li, C. Lian, Q. Luo, H. Tian and W. H. Zhu, *J. Am. Chem. Soc.*, 2019, **141**, 18467–18474.
38 K. Higashiguchi, K. Matsuda, S. Kobatake, T. Yamada, T. Kawai and M. Irie, *Bull. Chem. Soc. Jpn.*, 2000, **73**, 2389–2394.
39 M. Kathan, F. Eisenreich, C. Jurissek, A. Dallmann, J. Gurke and S. Hecht, *Nat. Chem.*, 2018, **10**, 1031–1036.
40 S. Fredrich, A. Bonasera, V. Valderrey and S. Hecht, *J. Am. Chem. Soc.*, 2018, **140**, 6432–6440.
41 S. Kobatake, H. Imagawa, H. Nakatani and S. Nakashima, *New J. Chem.*, 2009, **33**, 1362–1367.
42 M. Herder, B. M. Schmidt, L. Grubert, M. Patzel, J. Schwarz and S. Hecht, *J. Am. Chem. Soc.*, 2015, **137**, 2738–2747.
43 M. Irie, T. Lifka, K. Uchida, S. Kobatake and Y. Shindo, *Chem. Commun.*, 1999, 747–748.
44 J. H. Day, *Chem. Rev.*, 1953, **53**, 167–189.
45 M. Irie, *Chem. Rev.*, 2000, **100**, 1685–1716.
46 H. Tian and S. J. Yang, *Chem. Soc. Rev.*, 2004, **33**, 85–97.
47 P. R. Hania, A. Pugzlys, L. N. Lucas, J. J. D. de Jong, B. L. Feringa, J. H. van Esch, H. T. Jonkman and K. Duppen, *J. Phys. Chem. A*, 2005, **109**, 9437–9442.
48 A. Jarota, E. Pastorczak and H. Abramczyk, *Phys. Chem. Chem. Phys.*, 2020, **22**, 5408–5412.
49 M. Isegawa and K. Morokuma, *J. Phys. Chem. A*, 2015, **119**, 4191–4199.
50 M. Boggio-Pasqua, M. Ravaglia, M. J. Bearpark, M. Garavelli and M. A. Robb, *J. Phys. Chem. A*, 2003, **107**, 11139–11152.
51 E. Runge and E. K. U. Gross, *Phys. Rev. Lett.*, 1984, **52**, 997–1000.
52 A. Dreuw and M. Head-Gordon, *Chem. Rev.*, 2005, **105**, 4009–4037.
53 J. D. Chai and M. Head-Gordon, *Phys. Chem. Chem. Phys.*, 2008, **10**, 6615–6620.
54 S. Miertus, E. Scrocco and J. Tomasi, *Chem. Phys.*, 1981, **55**, 117–129.
55 Y. H. Shao, M. Head-Gordon and A. I. Krylov, *J. Chem. Phys.*, 2003, **118**, 4807–4818.
56 M. Isegawa, R. Peverati and D. G. Truhlar, *J. Chem. Phys.*, 2012, **137**, 244104.
57 Y. H. Shao, Y. Mei, D. Sundholm and V. R. I. Kaila, *J. Chem. Theory Comput.*, 2020, **16**, 587–600.
58 S. M. Büllmann, T. Kolmar, P. Slawetzky, S. Wald and A. Jäschke, *Chem. Commun.*, 2021, **57**, 6596–6599.
59 T. Kolmar, S. M. Büllmann, C. Sarter, K. Höfer and A. Jäschke, *Angew. Chem., Int. Ed.*, 2021, **60**, 8164–8173.
60 D. L. Kellis, C. Sarter, B. L. Cannon, P. H. Davis, E. Graugnard, J. Lee, R. D. Pensack, T. Kolmar, A. Jäschke, B. Yurke and W. B. Knowlton, *ACS Nano*, 2019, **13**, 2986–2994.